# ELIMINATION OF CAVITATION-RELATED INSTABILITIES AND DAMAGE IN HIGH-ENERGY PUMP IMPELLERS

by

**Paul Cooper**

**Director, Research and Development, Pump Group**

**Donald P. Sloteman**

**Manager, Pump Research and Development, Pump Group**

**Edward Graf**

**Supervisor of Fluid Dynamics and Acoustics, Research Development, Pump Group**

**Ingersoll-Rand Company**

**Phillipsburg, New Jersey**

**and**

**Dirk J. Vlaming**

**Retired Senior Rotating Equipment Specialist**

**The Hague, Netherlands**

*Paul Cooper is Director of Research and Development for the Pump Group of Ingersoll-Rand Company, Phillipsburg, New Jersey. His responsibilities are the development of new pump products along with the hydraulic and acoustical improvement of centrifugal pumps.*

*Dr. Cooper joined Ingersoll-Rand's research center in Princeton in 1977, where he conducted research on pumps and turbines. Prior to that, he had hydraulic design responsibility for aircraft fuel and oil field pumps at TRW, Incorporated.*

*Dr. Cooper received a B.S. degree in Mechanical Engineering (1957) from Drexel University, an M.S. degree (1959) from Massachusetts Institute of Technology, and a Ph.D. (1972) from Case Western Reserve University. Dr. Cooper is a Fellow of the ASME, having served as chairman of the ASME Fluids Engineering Division. He is the author of several technical papers and reports on pump hydraulics and regularly lectures in this subject area. He currently serves on the Board of Directors of the Research and Development Council of New Jersey., and on the International Pump Users Symposium Advisory Committee.*

*Donald P. Sloteman is Manager of Pump Research and Development for the Inersoll-Rand Pump Group, located in Phillipsburg, New Jersey. His responsibilities include managing various Research and Development projects in the areas of new product development, product improvement, and advanced pump technology. He has been associated with a variety of programs which have included the development of high-speed inducers and pumps, backflow recirculators, power recovery turbines, cavitation resistant impellers, centrifugal slurry pumps, and research into the nature of impeller/diffuser interaction. He has conducted research programs funded by EPRI, NASA, and the U.S. Department of Energy. Before joining the Pump Group, he was employed at Ingersoll-Rand's Research Center in Princeton, New Jersey.*

*Mr. Sloteman received his B.S. in Mechanical Engineering from Drexel University and is a member of the ASME.*

*Edward Graf is Supervisor of Fluid Dynamics and Acoustics, Pump Group Research and Development Pump Group Ingersoll-Rand Company, Phillipsburg, New Jersey. His primary responsibilities are adapting sophisticated codes to the hydraulic and accoustic design and analysis of high energy industrial pumps and super-quiet pumps for Navy submarine applications.*

*Mr. Graf joined Ingersoll-Rand with the Turbo Division group in 1981, during which time he had primary responsibility for the aerodynamic design of all advanced axial flow turbomachinery, including compressors, power turbines and hot gas expanders.*

*Previously, Mr. Graf was employed as a Senior Engineer with the Westinghouse Electric Corporation with responsibility for the aerodynamic design of turbomachinery for specialized applications.*

*Mr. Graf received his BSME degree at the University of Pennsylvania and his MSME at the California Institute of Technology. He is a member of the ASME and a licensed Professional Engineer in the State of Pennsylvania.*

## ABSTRACT

The suction-stage impeller of a large crude oil pipeline pump was designed by combining quasi-three dimensional flow analysis with current theories to generate an impeller geometry, which was evaluated in a half-size model test pump. The model impeller was compared to a reference impeller designed in accordance with principles derived from correlations of field

data to resist cavitation erosion for 40,000 hours. Flow visualization testing showed the model impeller to be free of bubbles and other cavities from 80 percent to 120 percent of rated flow and to have substantially less two-phase flow activity than the reference impeller over the required flow rate range from 50 percent to 135 percent. Measurements of pressure pulsations, cavitation noise level and soft coating removal, in addition to the visual observations, demonstrated that the model impeller design has not only greater erosion resistance than the reference impeller, but that the design also produces significantly less mechanical response of the pump and surrounding structures to cavity oscillations in the flow passages.

## INTRODUCTION

A major concern for designers and users of high-energy centrifugal pumping machinery is the potential for interaction of two-phase flow phenomena with the mechanical and material response mechanisms of the pumping elements. These interactions take the form of material erosion of the suction stages of the pump, excitation of the rotor and casing caused by the resulting fluctuating cavity behavior, and the generation of piping vibration and movement. The severity of these responses, which can lead to failure of pump and system components, depends on the so-called energy level of the pump. This level can be quantified in terms of the stresses developed at critical locations within the pump and which are directly connected with the pressure rise or head of the stage involved. The critical or limiting value of this head for typical centrifugal pump geometries decreases with increasing specific speed [1].

Similarly, the rate of cavitation erosion within the impeller increases with stage head or, more directly, with the NPSH, a fraction of that head. In particular, studies indicate that for a given ratio R of available NPSH to that required to maintain pump head (NPSHA/NPSHR), the rate of erosion depth penetration varies approximately with the cube of the NPSH. Since this NPSH is proportional to the square of $U_e$, the erosion rate varies with about the sixth power of impeller inlet blade tip speed $U_e$ [2, 3].

Connected with the phenomenon of cavitation is the fact that the motion, volume and extent of bubbles and other cavities are generally unsteady [4], a characteristic revealed in flow visualization studies of pump impeller inlet regions [5, 6]. This unsteadiness arises from the unstable interaction between the cavity configuration and the developing blade load. The greater pressure near the cavity closure point tends to collapse the cavity, which increases the blade loading toward the leading edge of the blade. This in turn lowers the suction-side pressure and re-establishes a longer cavity. The resulting oscillating cavitation occurs as the flow rate is reduced below the point of best efficiency or BEP (because of the attendant greater angle of attack) and increases in frequency with the R-value [7].

Oscillating cavities block the flow passages of the impeller and cause momentary reductions in pump head. The consequent pressure-rise fluctuations do not affect all the passages at the same instant and so give rise to fluctuating loads on the impeller. The resultant unit loading on the radial bearings, for instance, is shown in Figure 1 (for journal bearings), to be associated with the pump stage pressure rise, the value of this loading being another way of quantifying the energy level of the pump. Again the limiting value of this pressure rise for a given value of the energy level defined in this way decreases with increasing specific speed [1]. (The development that leads to the plots of Figure 1 is contained in the APPENDIX.)

The fluctuating pressure loadings at the impeller periphery of the first stage, which give rise to these unit loads in the radial bearings, also cause axial load fluctuations because the typical

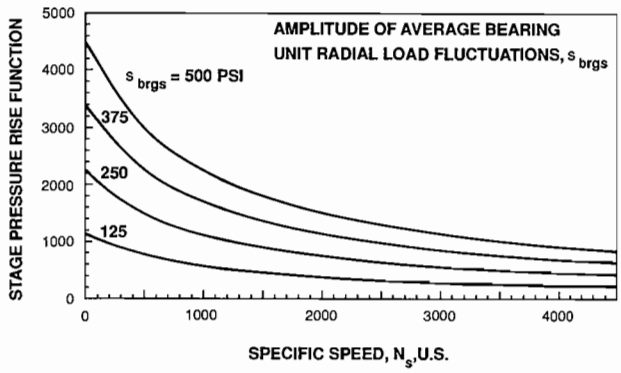


*Figure 1. Effects of Cavitation-related Instabilities Occurring in High-Energy Pumps. The relation of stage pressure rise to fluctuating radial load on journal bearings caused by oscillating cavitation (APPENDIX 1).*

multistage pump impeller is not of itself hydraulically thrust-balanced. Furthermore, unsteady cavitation surge, occurring at off-design low flowrates, has been shown to produce fluctuating axial loads because of variations in the radial distributions of pressure across the eye of the impeller [8]. The consequent vibratory axial movement of the impeller has led to seal and bearing failures [9].

It became necessary to quantify the foregoing phenomena in order to design a large pipeline pump that would be assured of operating reliably in the field for an acceptable period of time. Specifically, this pump was required to produce 2,000 ft of head in 0.824-specific gravity crude oil at a rated flow of 46,850 USgpm. Running at 2,300 rpm, the machine consists of two parallel two-stage volute pumps on a common shaft in the same casing. An isometric view of the full-scale prototype is shown in Figure 2. The required performance of this pump, which includes operating over a flow rate range from 50 percent to 135 percent of rated flow at a constant available NPSH of 238 ft, is shown in Figure 3. In addition to this performance, the pump was required to resist cavitation attack for a period of 40,000 hr. A look at the available theories for cavitation damage revealed missing links, which made an analytical prediction of

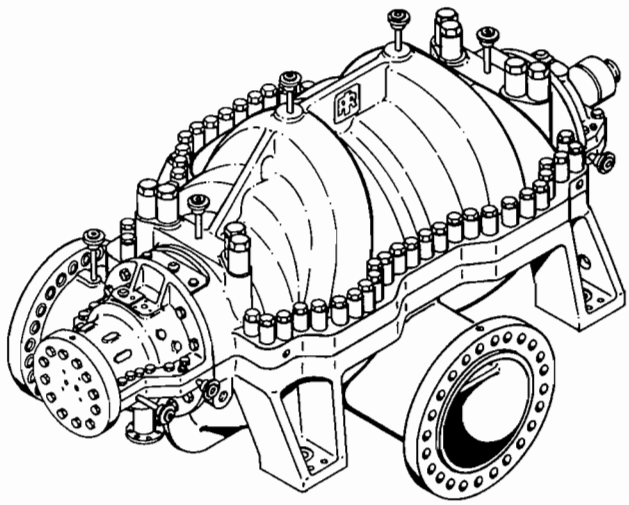

*Figure 2. 24x28 DA Pipeline Pump. This 25,000 hp oil pipeline pump utilizes two suction impellers, each with its own inlet, on either end of the pump shaft. Two second-stage impellers discharge to a common outlet.*

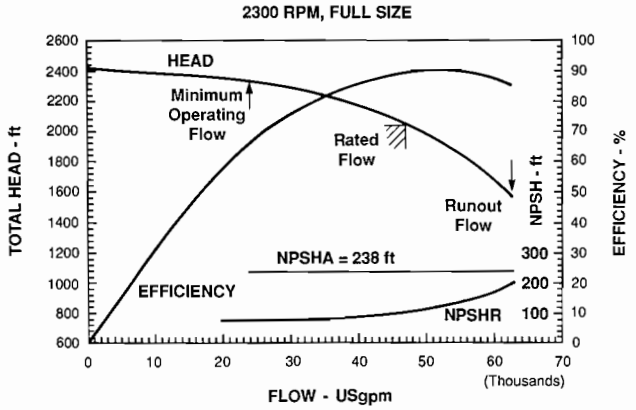


*Figure 3. 24x28 DA Performance Curve. Proposed performance of the 24x28 DA pipeline pump, including customer specified performance requirements.*

life uncertain. The customer had requested that criteria be developed for acceptance of the design from a life standpoint via flow visualization of a model of one of the two identical suction stages.

To develop the needed criteria, the researchers recognized that field data from pump installations had been studied and correlated to yield a set of guidelines for designing the inlet region of an impeller which would last for the required 40,000 hr. This was the work of one of the authors, in which he gave empirical formulas for calculating the NPSH required over the entire flowrate range [10]. If they were to design an impeller in accordance with these guidelines, they could be reasonably sure that it would last for 40,000 hr, at least from a cavitation erosion standpoint. Whatever two-phase flow activity this impeller would produce in the required flow visualization test, therefore, would be acceptable. But the customer wanted the manufacturer also to minimize the vapor volume within the impeller to avoid the aforementioned unsteadiness and fluctuating load response. Therefore, the researchers set a two-fold goal for the model acceptance testing: a) the model impeller should evidence less vapor volume, cavitation noise level, soft coating removal and pressure pulsations than a reference impeller designed in accordance with the above guidelines; and b) the model impeller should be bubble-free (no cavities) over as wide as possible a portion of the required flowrate range—the rated point being centered in this range.

The authors believed that if they concentrated on meeting goal (b), they also would satisfy goal (a). To that end, they needed to verify analytically that their design would not produce reductions of static pressure below the vapor pressure of the liquid within the blade system—an approach developed in recent years and which has led to minimum vapor formation and blockage of the impeller passages in these and other efforts [11]. For the current task, therefore, they used the single-phase, quasi-three-dimensional flow computer codes developed by NASA, which are widely recognized and used for impeller design work [12, 13]. Of course, the final arbiter of this design effort would be the flow visualization testing and whether the impeller met the established conditions.

## THEORY AND DESIGN

The operating requirements of the full-scale pump with which this study deals are given in Table 1. In order to achieve optimum pump performance over the range of 50 percent to 135 percent of the rated flow, the best efficiency of the pump was selected to occur at a flowrate nine percent greater than the rated flow of 46,850 USgpm or 23,425 USgpm for each impeller. This made the required maximum flowrate equal to 124 percent of that BEP. Selection of impeller hub/shroud profile, exit angle and volute design was based on existing models.

*Table 1. Operating and Design Conditions.*

| Quantity | Full-scale Impeller | Model Impeller | Reference Impeller |
|---|---|---|---|
| Scale, % | 100 | 50 | 50 |
| Speed, N, rpm | 2,300 | 1,800 | 1,800 |
| Rated flow, $Q_r$, USgpm | 23,425 | 2,292 | 2,292 |
| Best efficiency flow, $Q_{bep}$ | | | |
| USgpm | 25,500 | 2,495 | 2,495 |
| % of $Q_r$ | 109 | 109 | 109 |
| Minimum flow, $Q_{min}$ | | | |
| % of $Q_r$ | 50 | 50 | 50 |
| % of $Q_{bep}$ | 46 | 46 | 46 |
| Maximum flow, $Q_{max}$ | | | |
| % of $Q_r$ | 135 | 135 | 135 |
| % of $Q_{bep}$ | 124 | 124 | 124 |
| NPSH available, ft. | 238 | 36.5 | 36.5 |

### *Reference Impeller*

The next step was to design the reference impeller, first by optimizing the inlet geometry to a) minimize the flowrate $Q_{mu}$ at which recirculation creates unacceptable hydraulic/mechanical interactions and b) produce a 40,000-hour-life NPSH requirement that does not exceed the available NPSH over the required flow range from minimum to maximum, as specified in Table 1. This optimization process was carried out, as outlined by Vlaming, and the obtained results for the eye diameter $D_e$ and related data are given in Table 2.

*Table 2. Design Data for Half-Scale Impellers (applicable to both reference and model impellers).*

| | |
|---|---|
| Eye diameter, $D_e$, in. | 8.38 |
| Shaft diameter, $D_s$, in. | 4.3125 |
| Exit diameter, $D_2$, in. | 13.5 |
| Blade inlet tip speed, $U_e$, ft/sec (Full scale: 168.2 ft/sec) | 65.8 |
| Inlet flow coefficient at BEP, $\phi = \{Q_{bep}/[(\pi/4)(D_e^2 - D_s^2)]\}/U_e$ | 0.3 |
| Available NPSH-coefficient, $= NPSHA/(U_e^2/2g)$ | 0.542 |
| Specific speed | |
| U.S. units | 2097 |
| Universal $[= \Omega Q^{1/2}/(gH)^{3/4}]$ | 0.767 |
| Pump flow rate at which suction recirculation occurs, $Q_{sr}$ | 0.624 $Q_r$ |
| Minimum allowable flow rate, $Q_{ma}$ | 0.381 $Q_r$ |

As discussed further on, this process also involved the choice of a shockless entry flowrate $Q_{sc}$ that was seven percent greater than the BEP flowrate $Q_{bep}$. The researchers then found the blade inlet camberline angles at hub and shroud, using the relationships specified in his recent paper [10], modified to account for the prewhirl generated by the suction approach chamber.

### *Recirculation*

It can be seen from Table 2 that $D_e > 0.5\, D_2$; so, as the pump flowrate is reduced, suction recirculation can be expected to occur before

discharge recirculation [14]. Thus, the eye needed to be as small as possible to minimize the flowrate $Q_{sr}$, below which fluid recirculates out of the impeller eye. This necessity can be deduced from the empirical relationship

$$Q_{sr} = \pi \Omega r_e^3 [1-(D_s/D_e)^2] \phi_{sr} \quad (1)$$

where the suction recirculation flow coefficient

$$\phi_{sr} = \tan\beta_e [1-0.2091(\beta_e - 9.5)^{.4}] \quad (2)$$

is Gopalakrishnan's version [14] of an earlier development by Fraser [15], and $\beta_e$ is the blade inlet angle (deg) at the shroud. Except at the highest energy levels $Q < Q_{sr}$ does not necessarily result in injurious mechanical response of the pump, as indicated by the expression for minimum allowable flowrate, $Q_{ma}$ [14]:

$$Q_{ma} = K_1 \quad K_2 \quad K_3 \quad K_4 \quad K_5 \quad Q_{sr} \quad (3)$$

where the Ks are defined in [14] and conservatively are taken to be unity except that

$$K_2 = \text{Specific Gravity of Fluid} = 0.824, \text{ and}$$

$$K_3 = (\text{NPSHA/NPSHR}) - \text{effect} = 0.74,$$

yielding $Q_{ma} = 0.381\ Q_r$ as given in Table 2. This is less than the minimum required flowrate $Q_{min}$ of 0.5 $Q_r$ from Table 1, indicating that, at the energy level of this pump, operability should be satisfactory within the required range of flowrate Q.

These results were computed for the reference impeller. Equations (1) and (3) would yield smaller values for $Q_{sr}$ and $Q_{ma}$ in the case of the model impeller, because smaller values of $\beta_e$ were used in that impeller. This will be apparent in the following discussion for the reference impeller and in the subsequent section on the model impeller. However, these empirical equations are probably not applicable for the unusual blade shape described in that section. Therefore, in preparing Table 2, the authors conservatively assumed tht these values for $Q_{sr}$ and $Q_{ma}$ apply to both refenence and model impellers.

*Resistance to Cavitation Damage—NPSHR*

The eye-optimization process produced a requirement for the NPSH necessary for the impeller to resist attack by cavitation for 40,000 hr - here called "$NPSH_{40}$", as opposed to the NPSHR curve in Figure 3. As seen in Figure 4, there still is a slight margin between $NPSH_{40}$ and NPSHA at both the minimum and maximum specified flowrates. That this margin is nearly the same at these two ends of the range is a consequence of the eye optimization process, which in turn is consonant with the choice of 1.07 for the ratio of the shockless entry flowrate to that at BEP. The characteristic V-shaped curve for $NPSH_{40}$ was computed from Vlaming's empirical Equations (10) written as follows:

$$NPSH_{40} = NPSH_{se} + \Delta NPSH, \quad (4)$$

where the shockless-entry component is

$$NPSH_{se} = C_a C_b C_c (U_e^2/2g)[(k_1+k_2)\tan^2\beta_e + k_2] \quad (5)$$

with $k_1 = 1.2$ and
$k_2 = 0.2334 + [U_e(\text{ft/sec})/400]^4 = 0.2646$

and the incidence effect is

$$\Delta NPSH = NPSH_{se} * (NPSH_{se}^{0.105} - 1) * f \quad (6)$$

where

$$f = \begin{cases} 0.887q + 0.893q^2 & \text{for } Q < Q_{se} \\ -2.82q + 6.61q^2 & \text{for } Q > Q_{se} \end{cases}$$

with

$$q = (Q_{se}/Q_{bep}) - (Q/Q_{bep})$$

With the specific speed and material constants $C_a$ and $C_c$ at unity and the pumped-fluid constant $C_b = 0.74$ for oil, $NPSH_{se}$ = 145.2 ft at full scale. Here, 19.45 degrees was used for the blade inlet angle at the shroud $\beta_e$. The actual value of $\beta_e$ was slightly larger to allow for the prewhirl generated by the suction approach chamber.

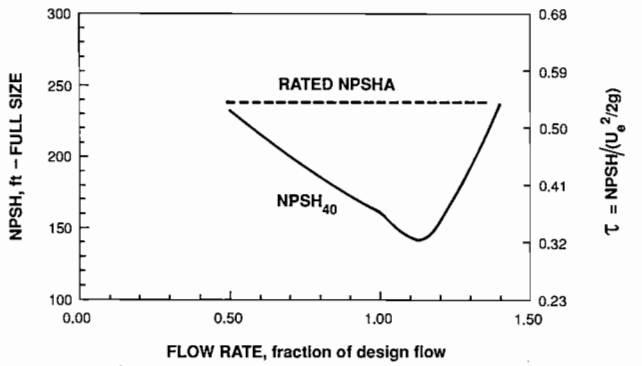


*Figure 4. NPSH Requirements to Achieve 40,000 Hr of Cavitation Life. This $NPSH_{40}$ was calculated from the empirical model developed by Vlaming [10], for the selected impeller inlet tip speed.*

*Cavity Length*

The recent EPRI-sponsored research work reported by Gulich predicts the rate of cavitation erosion depth penetration if the bubble or cavity length $L_{cav}$ is known [3]. Without that length information, one must rely on other empirical methods, such as that of Vlaming. Both the reference and model impellers had the same geometrical features so far as the EPRI method is concerned. This method states that a depth penetration of 75 percent of the blade thickness constitutes the end of the useful life of the impeller in question. Knowing the blade thickness, the researchers could back calculate from the following formula to find $L_{cav}$:

$$dE/dt = C(L_{cav}/L_{cav.ref})^n k_A^3 U_e^6 \rho_L^3 A/(8*TS^2) \quad (7)$$

where E = the erosion depth in mm
t = time in hours
$k_A = \tau_A - \phi^2$
and $\tau = NPSH/(U_e^2/2g)$, where $\tau_A$ corresponds to NPSHA and is dimensionless
$\phi$ = inlet flow coefficient defined in Table 2
n = 2.83 for suction side and 2.6 for pressure side
$\rho_L$ = liquid density = 824 kg/m$^3$ (corresponds to 0.824 specific gravity - for crude oil)
$U_e$ = Impeller inlet tip speed = 51.27 m/s.

$L_{cav,ref}$ = 10mm or 0.3937 in.
A = crude-oil correction = 0.261 (A = 1 for water)
TS = 860,000,000 Pa (corresponds to 125,000 psi - for CA6NM)

$$C = \begin{cases} 8.28 \times 10^{-6} \text{ (mm/hr)/Pa:} & \text{suction side} \\ 3.96 \times 10^{-4} \text{ (mm/hr)/Pa:} & \text{pressure side} \end{cases}$$

The authors applied Equation (7) in this way to the full-scale impeller and obtained the permissible cavity lengths to achieve a 40,000-hr life. By maintaining the same $\tau_A$-value on the half-size model and reference impellers, NPSHA = 36.5 ft (Table 1) and half-size cavities are obtained. Therefore, half the full-scale lengths found from Equation (7) are shown in Figure 5, for both suction and pressure sides of the impeller blades. These, in turn, must not be exceeded during the flow visualization testing if the required life is to be achieved at full-scale in crude oil.

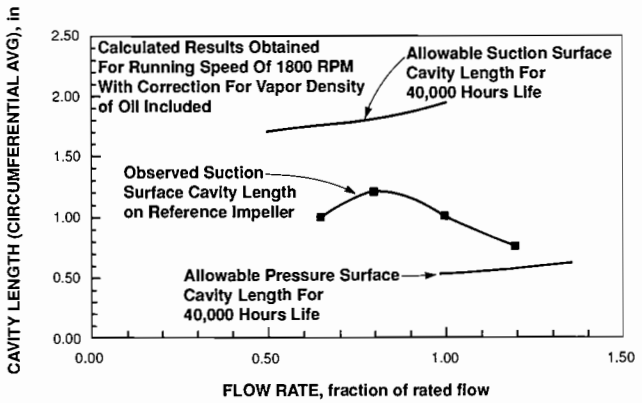


*Figure 5. Reference Impeller Cavity Length and EPRI Life Correlation. The cavitation erosion formulas [3], with corrections for oil included, when compared to the cavity lengths of the reference impeller, indicate a better than 40,000 hr cavitation life at the rated NPSH. The lack of any significant caviation activity in the model impeller would indicate even greater life.*

### *Relation of Damage to Cavity Length*

As already stated, the cavity length is assumed to be unknown analytically. However, in other EPRI-sponsored work, a method for computing the cavity length from the blade surface pressure distributions was developed [16]. This method needs to be correlated with experimental results and so was not used here. Furthermore, there are varying amounts of cavitation damage that can occur for the same cavity length. These relate to the actual number and sizes of bubbles collapsing on the blade surface within, or more precisely, at the downstream closure point of the cavity. Two extremes are observed here: a) If the closure zone is occupied by a cloud of bubbles, damage will occur there [17]. The vapor volume generation needed for these bubbles comes via evaporation from the cavity/liquid interface, which, in turn, is caused by a slight reduction in pressure within the cavity below the vapor pressure of the liquid [18]. Incidentally, the much smaller volume of vapor generated in crude oil produces less damage than does the much larger cold water volume [19]. b) On the other hand, if the cavity closes without the additional two-phase bubble activity, no damage is observed. In that case, the lack of vaporization from the cavity-liquid interface to supply collapsing bubbles would indicate a smaller pressure drop below vapor pressure within the cavity.

The geometry of cavity formation and closure undoubtedly governs which of these configurations (or combination thereof) exists. The data scatter found in the development of the cavity-length erosion model undoubtedly arose from the differences in closure configuration. This is a reason for introducing soft-coating removal tests in addition to flow visualization.

### *Oscillating Cavitation and Recirculation*

Further complications in the cavity-length approach become apparent as one observes the cavitating flow in the impeller eye region as the flowrate is reduced below that of the BEP. Again, there are two notable configurations: a) As noted earlier, the cavity that is reasonably steady and not fluctuating in length generally does the opposite in departing from the BEP, introducing the fluctuating loading described in conjunction with Figure 1. b) At lower flowrates, recirculation sets in, and the backflow destroys all semblance of a cavity. Instead, isolated bubbles can be seen forming in the interior of the liquid from the attendant vortical activity between the blades. At present, testing is the only way to determine erosion rates at such flow conditions. Here, the fluctuating loading persists, and is aggravated by the presence of two-phase flow.

### *Blade Loading Analysis*

The uncertainties in cavitation erosion rates and, more important, in the fluctuating loads accompanying cavitation, are best addressed by making an effort to remove all two-phase flow activity from the impeller. While the vortical interactions occurring in the recirculation mode occur at very high values of NPSH, oscillating cavitation should be removed simply by maintaining the computed pressure at a level above the vapor pressure on the blades. The quasi-three dimensional methods currently available are unable to deal with flow that is separated and mixing, but this inability poses less of a problem at flowrates above the recirculation value $Q_{sr}$. In this case, a design is required for which the presure p is greater then the vapor pressure $p_v$. The condition for this to hold is

$$\tau > -C_p \tag{8}$$

where

$$\tau = (P_o - p_v)/(\rho_L U_e^2/2) = \text{NPSHA}/(U_e^2/2g) \tag{9}$$

and the local pressure coefficient $C_p$ is given by

$$C_p = (p - P_o)/(\rho_L U_e^2/2) \tag{10}$$

and p is local static pressure; $P_o$ = upstream total pressure.

In Figure 6, the pressure coefficient distributions are shown on a blade of the reference impeller at the rated flow condition. While the researchers also obtained results at the hub and mean locations throughout the impeller, just the results along the shroud are shown, because that is where the relative velocities are greatest and, therefore, where small percentage variations in velocity produce significant pressure changes. In Figure 6, features shown are a) the complete distribution of $C_p$ along the shroud from inlet to outlet, and b) an amplified portion of (a) in the leading edge region. Details on the nose of the blade are not shown; however, it is clear that the negative excursion of $C_p$ is at least as great as the value of the NPSH coefficient $\tau_A$, which is equal to 0.542, (Table 2). Negligible improvement was found in this situation at other flowrates.

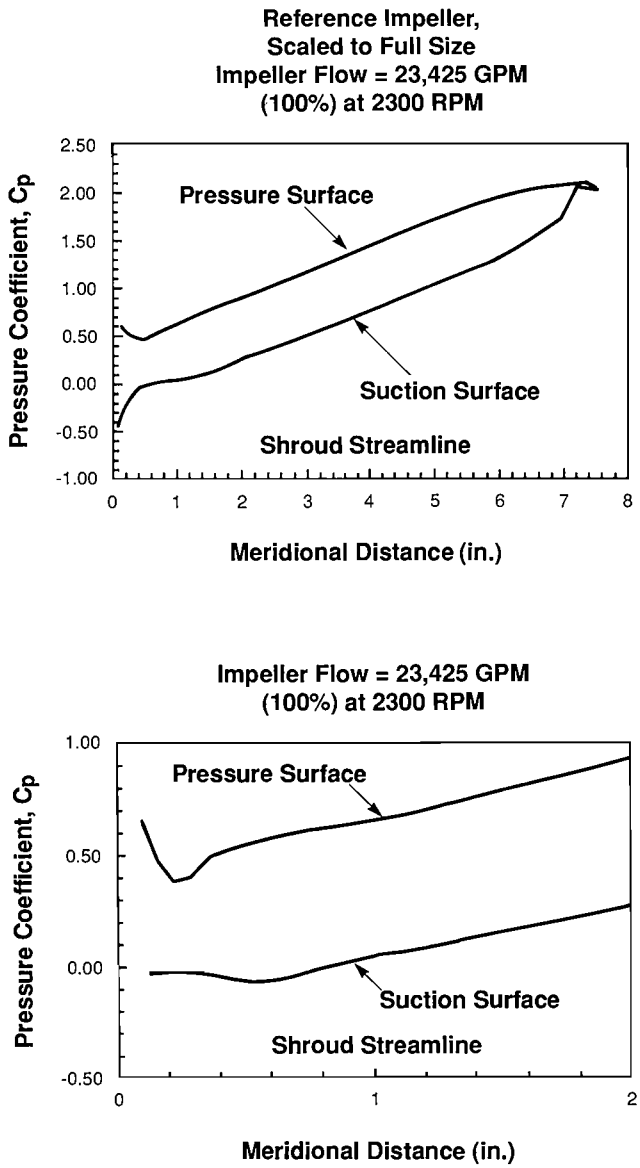


*Figure 6. Reference Impeller Blade Loading. The pressure coefficient distributions shown at the rated flow condition (100 percent) along the shroud streamline provide an indication of the potential for cavitation formation on the impeller blade surface. The top plot is for the complete passage from inlet to exit, and the bottom plot is a detail of the region near the leading edge.*

*The Model Impeller*

The method of designing the reference impeller was developed from existing design procedures. These procedures are an improvement over earlier practice in that correct angles of the blades at hub and shroud are required. However, these procedures do not incorporate the additional degrees of freedom in varying blade leading edge shape that must be exercised if Equation (8) is to be satisfied over a reasonable portion of the operating range. To do the latter for the model impeller, the blade angles were reduced along the leading edge below those employed for the reference impeller. But then leading edge shapes that are tapered [20] had to be introduced and a significant variation of blade camber angle had to be employed. This was necessary in order to maintain the opening between blades (at the inlet throat) so that NPSHR does not exceed the supplied NPSHA at the highest flowrate. Analytically, a blade shape was produced that was a marked improvement over the reference impeller. The results are shown in Figure 7, which is a series of amplified plots of $C_p$ in the leading edge region of the impeller for 80 percent, 100 percent and 120 percent of rated flow. A $C_p$ value that comes close to the negative of the supplied NPSHA as represented by $\tau = 0.542$ is observed in none of these cases. Looking at this series more closely, it is seen that the best result is at 100 percent flow, and that $C_p$ is becoming decidedly more negative at 80 percent flow. The situation at 120 percent flow is similar to the 80 percent case (as might be expected from the "V"-shape of Vlaming's curve in Figure 4). But, here, the roles of the pressure and suction sides of the blade are reversed, the lower pressure at the leading edge being on the pressure side. This is the negative-incidence situation expected as flow increases above that for which the leading edges were established.

The pressure distributions can be only an indication of what to expect in a test because of the influence of nose shape, roughness effects on cavitation inception and three-dimensional secondary flow patterns not analyzed in the quasi-three dimensional analysis used. Nevertheless, it is logical to pursue the goal of satisfying Equation (8) by whatever practical means at hand. It remains for flow visualization, soft coating and pressure pulsation testing to evaluate and further quantify this design approach.

## TEST APPROACH AND HARDWARE

The researchers conducted an experimental program in order to compare the reference and model impellers in a series of tests. These tests were structured to gauge the potential for cavitation life and two-phase stability of one impeller versus the other. These included cavitation bubble length, cavitation noise level, soft coating removal and pressure pulsation behavior. Meeting or exceeding the performance levels of the reference impeller in all of these areas should satisfy the user that the full-size first stage impeller, to be scaled up from the model impeller, will provide the desired performance levels.

The authors chose the model ratio to be 1:2. They considered this to be a practical size that would allow them to obtain the needed data rapidly and at reasonable cost without sacrificing the validity of the results. The bubble dynamics of the full size prototype and of the model should be similar when they are operated at identical values of dimensionless NPSH ($\tau$), since dynamic similarity then exists [3]. Modelling the gas content or particle distributions was not relevant since the researchers were concerned primarily with a comparison to the reference design. As mentioned earlier, geometric similarity was preserved in all the hydraulic passages of the first stage, up to the crossover to the second stage. A cross section of the test vehicle is shown in Figure 8. The authors gave special attention to the design of the transparent window assembly to assure full 360 degree visual access to the impeller eye. The inlet was cast from scaled-down drawings of the full-size hardware. To save cost and reduce lead time, they used a bearing and seal housing combination from standard production parts. This configuration places the impeller in an overhung position on a shaft supported by a single deep-groove ball bearing and a set of angular contact ball bearings outboard. Modelling of the rotordynamics was not a concern of this test program; the authors simply were evaluating the hydraulic performance and stability of the design. The model impeller was precision-investment cast from a pattern machined from coordinates used in the full size design. The reference impeller was fabricated via the same process by the same pattern maker and foundry.

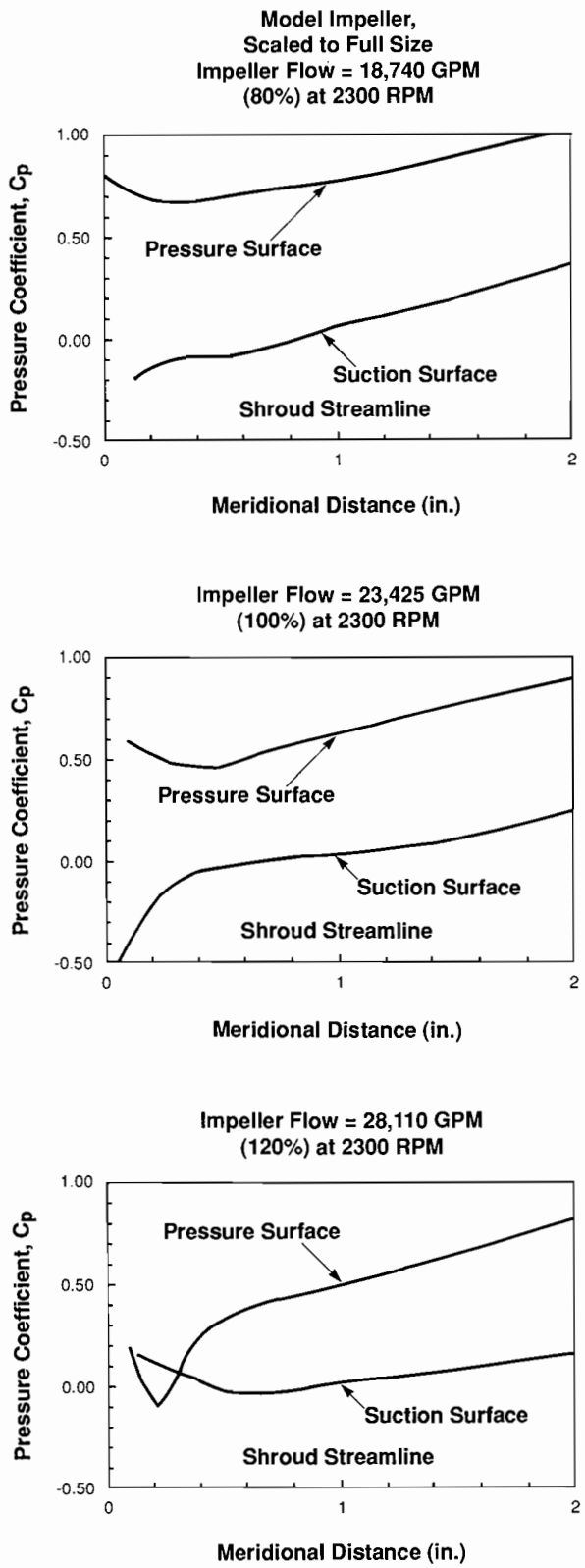


*Figure 7. Model Impeller Blade Loading. Pressure coefficient detail along shroud streamline near leading edge for 80 percent of rated flow (top); 100 percent (middle); 120 percent (bottom). Compare the middle plot with the leading edge detail plot in Figure 6. A significant increase in the minimum $C_p$ indicates reduced potential of cavitation activity on the blade surface.*

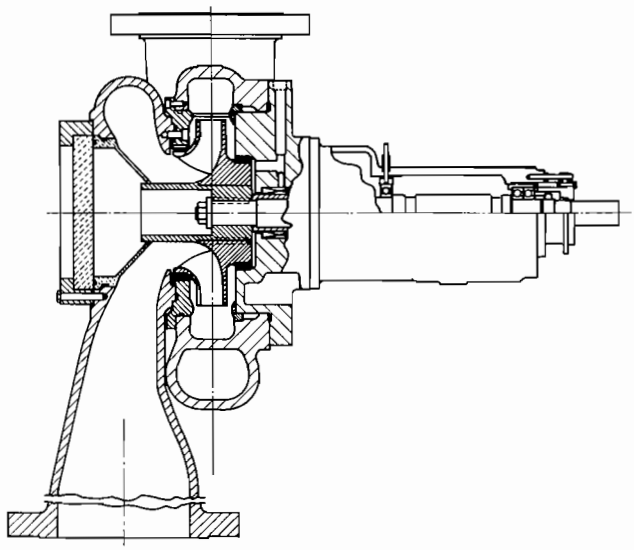

*Figure 8. Cross Section of Model Test Rig. Exact half-size models of the suction inlet, impeller and collector are used to verify performance of the full-size pump. Also shown is the two-piece, water flooded window, which provides full 360 degree visual access to the impeller eye.*

First, both impellers were tested over the specified flow range at the rated NPSHA (scaled to the half-size condition), visual observations were noted, video recordings were made of the bubble activity for later comparison, noise levels were measured and data were collected on pressure pulsations which were analyzed in real time. Later, a more detailed mapping of performance was conducted over the flow range specified, and for a wider range of NPSHA values. There was no difference in the hydraulic performance of the two impellers, except that the reference impeller had slightly more NPSHR-capability at flows greater than 120 percent of rated. A photograph of the test rig showing a representative selection of instrumentation used in the program appears in Figure 9. The results of this test work are presented in the following discussion.

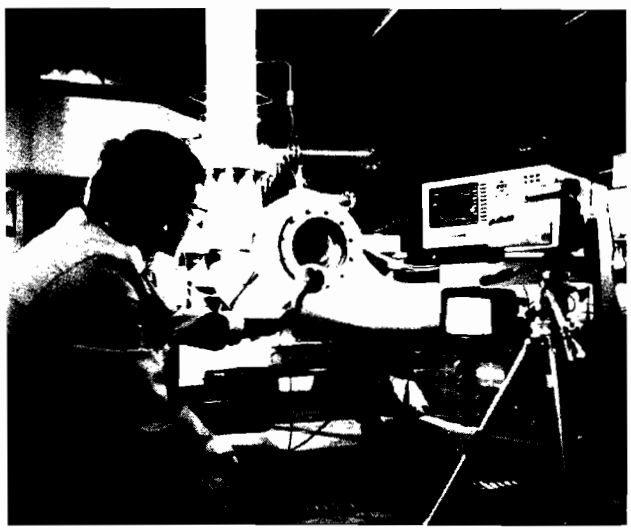

*Figure 9. Photo of Model Test Rig. The test rig and a portion of the instrumentation and video equipment used in documenting the performance of the reference and model impellers is shown in this photo.*

## TEST RESULTS

*Cavitation Bubble Behavior*

In their observations of two-phase flow within the test impellers, the authors identified the flows and NPSH values for which cavitation bubble behavior was present. The cavitation configurations typically were broken down into sheet cavitation, vortex cavitation and random, off-blade bubbles formed by the interaction of backflow with incoming flow [5].

The following series of photographs shows a comparison of cavitation bubble activity in the reference and model impellers. The photographs were taken with a 35mm camera equipped with a macrofocus lens, using a single flash strobe light (of one microsecond duration with a several-second recharge time required) to expose the film. The strobe fired only at one specific shaft position. This ensured that the same blade was illuminated for every exposure. Time delay circuitry was used to modify the trigger signal, if other blades were to be photographed. For visual observation, a lower energy strobe, capable of repetitive firings, was connected to the trigger circuit and flashed once per shaft revolution. This lower energy strobe was used for video documentation of bubble activity in the impeller.

Because of the design of the suction bay, a small region, in the vicinity of an inlet baffle prevents excessive swirl from developing upstream of the impeller. Preswirl counter to pump rotation exists in this region. This flow condition is a localized effect and, surprisingly, has little influence on the two-phase performance of the model impeller. The photographs were taken at a location that is 135 degrees from the baffle, in direction of rotation, where the average amount of preswirl produced by the suction bay is present. In a single photograph, the true dynamic nature of some of the cavitation behavior cannot be adequately expressed; so, to illustrate the presence of dynamic behavior, sometimes, more than one photo is included of a specific condition.

Only bubble activity on the suction side of the impeller blade is recorded and observed visually. Other tests are necessary to quantify activity on the hidden pressure surface.

The cavitation bubble formation on the reference impeller at 100 percent of rated flow and rated NPSHA is found in the two photos of Figure 10. These photos reveal a stable suction side cavity, about one inch long. By contrast, the model impeller is completely cavitation free at this condition, as seen in Figure 11. This is the result expected in view of the suction surface pressure coefficients plotted in Figures 6 and 7. In fact, the first observable bubble occured on the model impeller at a $\tau$ (or dimensionless NPSH) of 0.47 (the rated condition is $\tau = 0.54$). At rated NPSHA a well defined cavity was not formed on the model impeller blade until the flowrate was reduced below 80 percent.

As the flowrate was further reduced, the onset of suction recirculation was determined from the appearance of cavitation bubbles which were off the blade and upstream of the leading edges. These bubbles arose from the generation of vapor in the centers of flow vortices formed from the shearing of high velocity backflow and the lower energy through-flow approaching the impeller. Evidence of this behavior is seen on the reference impeller at about 75 percent of rated flow. The model impeller, with its flatter camberline angles, begins to recirculate between 60 percent and 70 percent of rated flow. The value of $Q_{sr}$ for the reference impeller is high, because the shockless entry flow is larger than typically encountered to achieve the large 135 percent runout flow condition (Table 1).

The two photographs of Figure 12 detail the unsteadiness of the bubble activity in the reference impeller at 50 percent flow, along with the presence of large amounts of vapor generated from the backflow. The fluctuation of the suction side cavity length is quite noticeable to the observer. By contrast, the vapor activity in the model impeller still appears quite benign (Figure 13). The suction side cavity activity is not as extensive as that

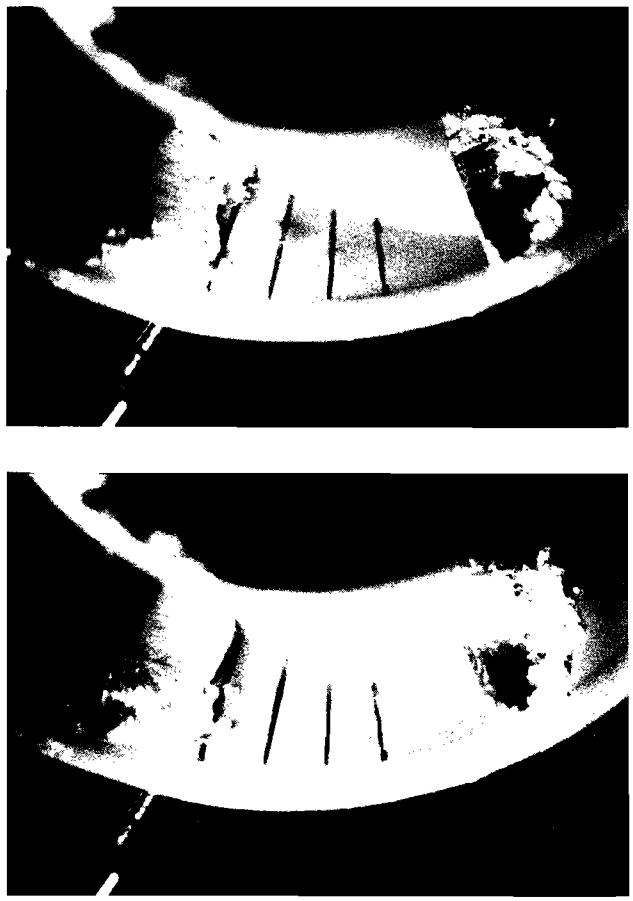

*Figure 10. Cavitation Bubble Activity of Reference Impeller at 100 percent Flow and Rated NPSH. The two photos, taken at the same flow condition at different instants of time, indicate a stable cavity (approximately one inch long) on the suction surface of the reference impeller.*

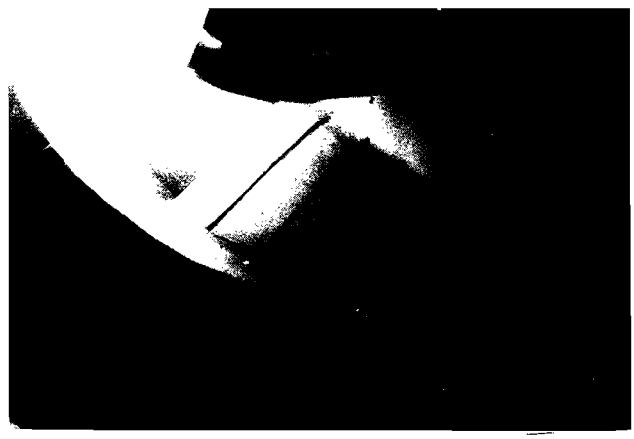

*Figure 11. Model Impeller Operating at 100 percent Flow and Rated NPSH. The model impeller provides cavitation-free operation at the rated flow and NPSH condition. This operating condition is identical to that shown in Figure 9.*

shown for the reference impeller. The presence of backflow-related vortex type cavitation is also observed, but since this impeller is not in as deep a state of recirculation as the reference wheel, the vortical behavior is not as severe. Based on these visual observations, it can be concluded that the blade design of the the model impeller, for which the suction surface pressure distribution at the design point was controlled, is still beneficial at off-design (where the flow field and cavitation behavior are heavily influenced by the recirculating fluid working its way upstream of the impeller).

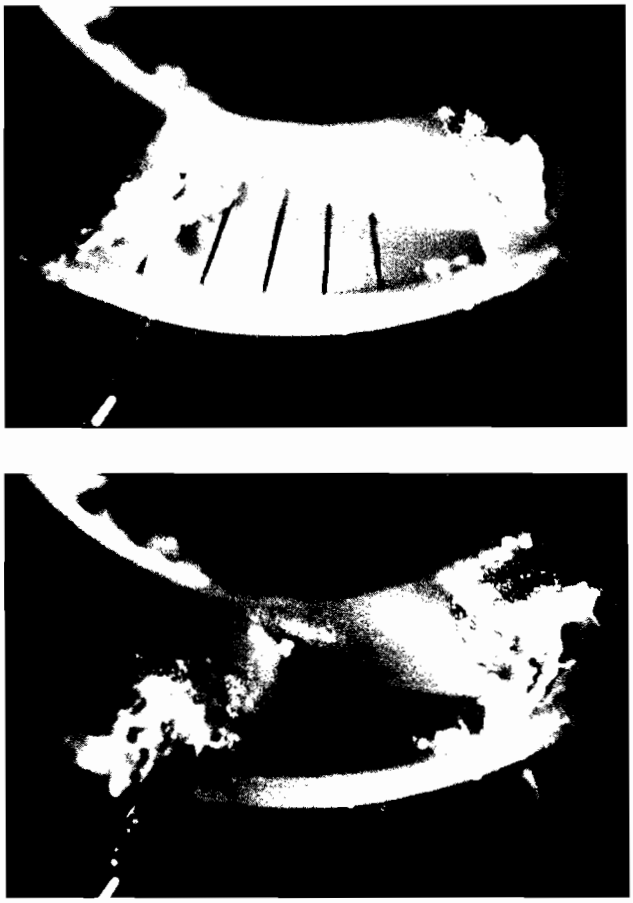

*Figure 12. Cavitation Activity in Reference Impeller Operating at 50 percent Flow and Rated NPSH. The unsteady nature of the cavitation bubble activity on the suction surface is observed from these two photos taken of the same operating conditions but at different instants. The cavitation activity here is heavily influenced by suction recirculation.*

At the runout condition of 135 percent of rated flow, the only visible bubble activity on the blade of the reference impeller occured in the region of negative preswirl. Slight traces of cavitation bubbles were evident on the model impeller as the blade passed through this region of the inlet.

From the observation that the model impeller generates less vapor volume and shorter (or nonexistent) suction side cavity lengths than the reference impeller, it can be concluded that the full-scale version of the model will exceed the 40,000 hr life criterion. Accompanying this conclusion, an assessment of the performance NPSH levels for both impellers is in order. A comparison is shown of the NPSH for three percent head fall-off (=NPSHR) in Figure 14. When the flowrate exceeds 120

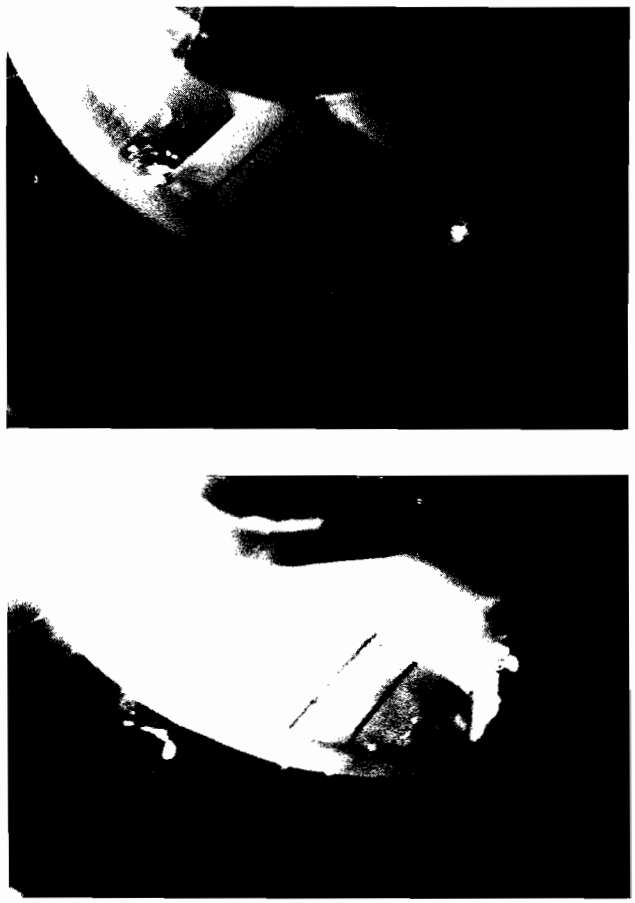

*Figure 13. Model Impeller Operating at 50 percent Flow and Rated NPSH. Suction recirculation is dominating the flow in the model impeller as it is the reference impeller. These two photos show cavitation activity (although much less than that found in the reference impeller) caused by the interaction of backflow with the incoming throughflow.*

percent, some reduction in the margin of R = NPSHA/NPSHR is experienced. At the runout condition, this ratio deteriorated to 1.04 for the model impeller *vs.* 1.22 for the reference wheel. Although this condition may appear marginal, the performance gains found in the new model impeller design outweigh this reduction in NPSH margin.

*Soft Coating Erosion*

Next, the damage potential was assessed of the various bubble patterns observed in the flow visualization phase of the test program—without resorting to expensive and time consuming material damage testing—by using a sacrificial coating on the test impellers. The coating material was a stencil ink used by the U.S. Navy in performing cavitation studies on ship propellers in the 1950s. This ink has been used successfully in several inhouse research programs. It has a weak enough bond with the impeller material so that when subjected to vapor-collapse pressure fields this bond can be broken in a short period of time. Removal of the coating was caused by the collapse of vapor cavities and not by any solubility effects in water. The zones of ink removal closely approximate actual zones of field damage.

The coating is applied uniformly and baked in an oven. The coated impeller is operated at a specified test condition for a

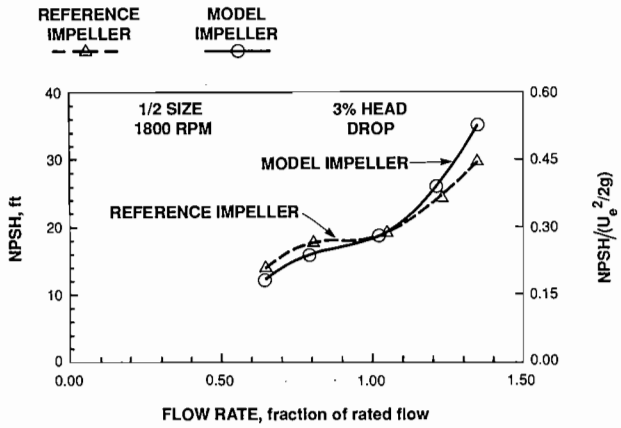


*Figure 14. Model and Reference Impeller Suction Performance. The NPSH required to supress a three percent drop in head is displayed for both impellers. At the runout flow the margin between the NPSHR and NPSHA is reduced more for the model impeller than the reference impeller. Suction performance at other flows is nearly identical.*

fixed period of time (typically one hour) and observations regarding coating removal are made. The coating is completely removed between tests and a fresh coat is applied for the next test condition. In this manner both impellers were evaluated for damage potential at a fixed operating condition, the measure of comparison being the area of ink removed.

The following sets of photographs (Figures 15, 16 and 17) enable the comparision of the coating removal of both impellers operating at identical flow conditions (rated NPSHA and flows of 50 percent, 100 percent and 135 percent of rated flow). The bubble patterns which caused these damage patterns were seen in earlier figures.

At 50 percent flow, both impellers have experienced slight ink removal at the inner diameter of the impeller eye (Figure 15). This is apparently caused by collapse of the backflow-caused bubbles present at this low flowrate. A dramatic difference between these two impellers exists at the hub, where a large area of ink has been removed from the reference impeller. This type of damage has been seen in the field on other applications. A word of caution is necessary when examining the extent of the area of ink removed at the hub. Referring to the bubble activity of Figure 12, notice that the length of the cavity at the hub never appears to match the extent of ink removed; although, the ink removed from the hub surface in a direction normal to the blade appears to match the vapor cavity thickness. It is possible that once the initiation of the coating removal begins, a peeling back of the coating occurs that is influenced more by fluid velocity than by actual effects of cavitation vapor collapse. Certainly, the flows at the cavity closure point are complex, are probably not parallel to the blade and may contribute to additional coating removal.

At 100 percent flow (Figure 16), the model impeller (bottom photo) shows no sign of ink removal, which is expected since it is operating bubble-free at this condition. The reference impeller still exhibits hub coating removal; although not as severe as it is at the lower flow condition. Here again, the caution just mentioned with regard to this damage zone still applies. It should also be noted that no suction surface ink removal has taken place on the reference impeller, even though a distinct cavity exists. Possibly longer running time is required to cause the coating bond to be broken. It must be kept in mind that the reference impeller is based on a design philosophy which has

*Figure 15. Comparison of Soft Coating Removal at 50 percent Flow and Rated NPSH. Significant ink removal at the hub is observed on the reference impeller, but not on the model impeller. Some ink removal has occurred at the inside diameter of the eye, for both impellers, due to backflow-generated cavitation bubble collapse at this location. See Figures 11 and 12 for the corresponding bubble activity.*

evolved from experience with 40,000 hr-life impellers, in which at the bubble conditions found on the reference impeller in Figure 10 do not result in excessive damage. The bubble free operation of the model impeller does suggest a cavitation life far in excess of 40,000 hr if operated exclusively near this flow condition.

At 135 percent flow, both impellers exhibit some signs of ink removal at the inner diameter of the inlet eye. The reference impeller has a damage zone on the suction surface, near the shroud (Figure 17). The high flow condition provokes some bubble activity on the inner diameter of the inlet bay, where the flow turns from a radial to axial direction. This cavitation is not caused by the impeller, but by the turning of the high-velocity fluid associated with this runout condition. The cavitation is observed to extend into the impeller with some potential for damage being apparent. Extended operation of either impeller at this runout condition would probably result in a reduced life limit arising from this cavitation.

Comparison of the two impellers on the basis of soft-coating removal tests indicate that the model impeller can be expected to achieve a longer cavitation life than the 40,000 hr reference impeller. Several more evaluations can be made to assess the damage potential for both impellers.

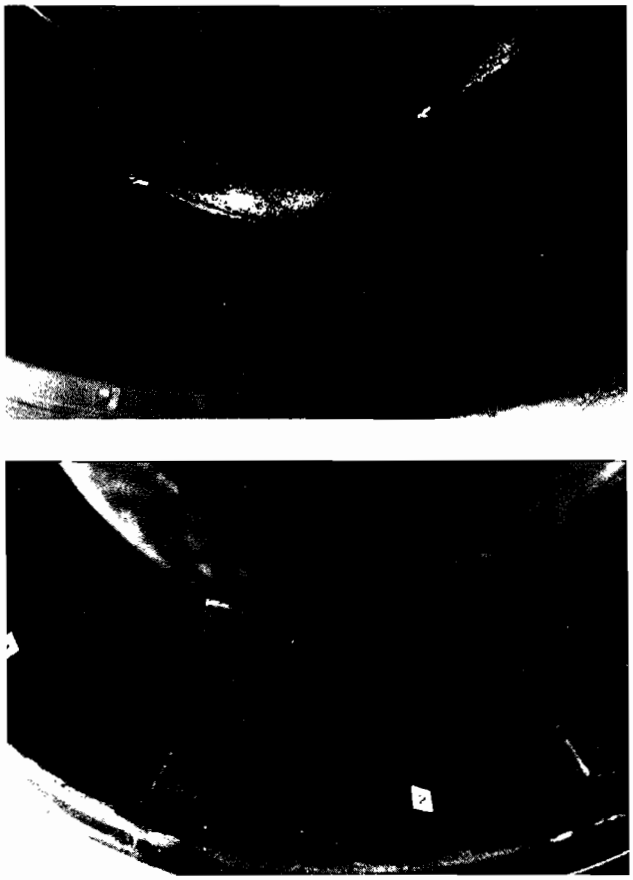

*Figure 16. Comparison of Soft Coating Removal at 100 percent Flow and Rated NPSH. Significant ink removal is still occurring at the hub of the reference impeller. No suction surface ink removal is seen, suggesting that longer test times may be necessary to obtain wear patterns at the cavity closure point. No ink removal is observed on the model impleller, which is to be expected since the impeller is cavitation-free at this condition.*

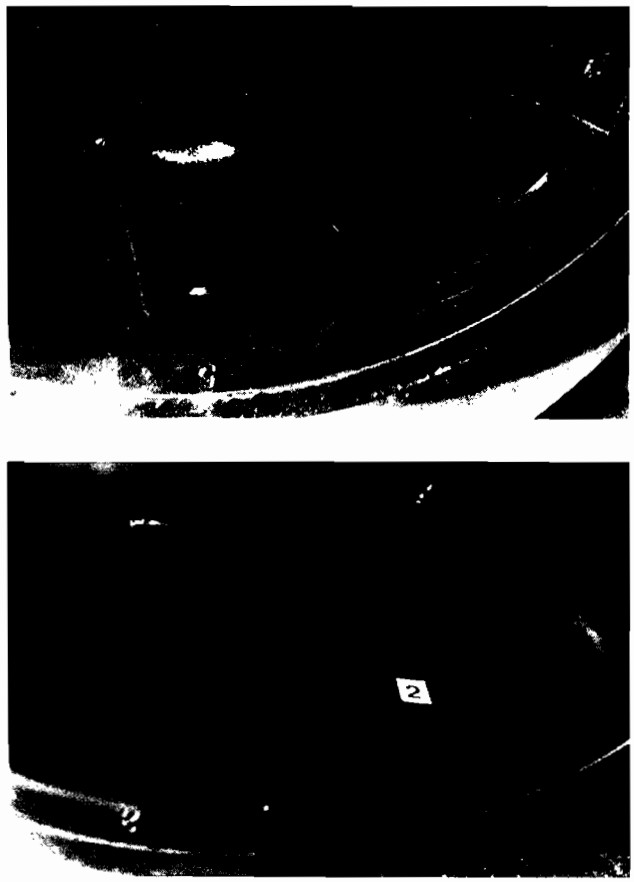

*Figure 17. Comparison of Soft Coating Removal at 135 percent Flow and Rated NPSH. Ink removal is still found on the reference impeller. The slight ink removal at the tip of the impeller is caused by cavitation generated by the high velocities present at the turn into the impeller eye from the suction inlet. This condition exists only at this extreme flow condition and can be found on both model and referece impellers.*

*Observed Cavity Lengths*

In the preceding section, *Theory and Design,* the authors computed the allowable cavity length for 40,000 hr of life in resistance to cavitation damage [3]. The results were plotted in Figure 5. Also shown in this figure are the lengths that were observed in the flow visualization testing of the reference impeller at rated NPSHA. The observed cavity lengths on the suction surface fall well below the calculated, allowable lengths at the rated NPSHA. Cavity lengths for the model impeller were either non-existent or significantly shorter than those observed on the reference impeller.

The researchers attempted to determine possible lengths of the pressure-side cavity via the soft-coating tests. The researchers expected that the cavity closure point should occur at the maximum extent of cavity length and that at this closure point, the ink would be removed. They observed no coating removal for either impeller (at any flowrate) from the pressure side. Possibly longer test times (than the one hour used for tests on the suction side) would produce some coating removal.

*Cavitation Noise Level*

The increase in fluid-borne noise levels occurring when a pump is experiencing cavitating flow has been reported widely in literature [3, 5, 21]. In fact attempts have even been made to correlate the damage rate with noise levels [3]. This test program offered the opportunity for the researchers to measure the cavitation noise levels and compare them to observed cavitation behavior in the impeller at various flow conditions. By using a hydrophone located in the suction inlet bay of the model, the fluid borne noise spectrum was measured up to 25 khz, over the entire flow range, for both reference and model impellers.

Under cavitating conditions, noise levels in the pump increase, as a result of the interaction of the collapse of cavitation bubbles with the surrounding fluid and structural components. The wide range of frequencies is associated with bubbles of various sizes. The collapse process produces pressure waves in the fluid and excites the surrounding structure, producing a wide range of resonances in the piping, rotor and pump casing. The vibration of these components in turn is transmitted back to the fluid in the form of small amplitude pressure pulsations. This contributes to an increase in the broadband pulsation spectrum, expressed logarithmically in terms of decibels referenced to some known pressure level. Comparing the levels of the noise spectra for different impellers or different operating conditions may lead to conclusions regarding the energy associated with the collapse of cavitation bubbles, but assessing the amount (or area) of damage done to the material may be difficult.

The two spectra shown in Figure 18 are of the reference impeller (top) and the model impeller (bottom) at 100 percent flow and rated NPSHA. A difference of about 20 dB is measured between the broadband amplitude levels. This is is the difference between the bubble activity of the reference impeller and the bubble-free operation of the model impeller found in Figures 10 and 11. The two spectra plotted in Figure 19 were obtained with the impellers operating at 50 percent flow and rated NPSHA; (see Figures 12 and 13 for the bubble activity occurring at this condition). The broadband noise levels appear to be equal in amplitude for this condition in spite of the large differences in vapor volume and vapor activity. The damage potential (as indicated from the soft coating tests) is also different for the two impellers at this flow condition. Thus, using noise level to assess damage potential is not an exact technique; however, it is still effective in identifying the presence of cavitation in the machine.

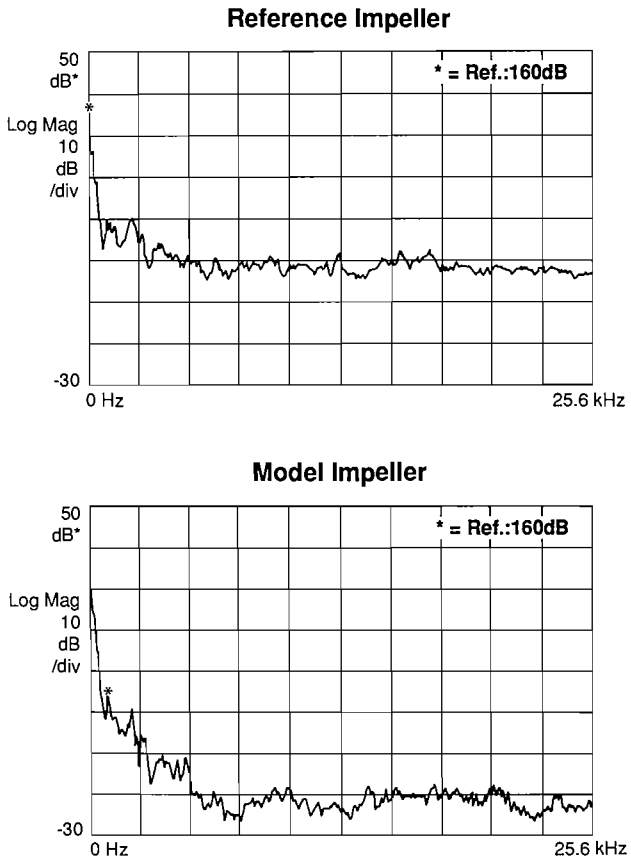


*Figure 18. Fluid-borne Noise Spectra for Reference and Model Impellers at 100 percent Flow. The bottom noise spectrum, of the model impeller, show an 18 db noise reduction due to cavitation free operation.*

A comparison of the broadband noise levels over the required flow range for the reference and model impellers is plotted in Figure 20. The 18-20 db reduction in noise for the model impeller at 100 percent flow disappears at the two extremes of operating flow range. The low flow condition has already been discussed, but the runout flow appears to indicate slightly higher noise levels in the model impeller. It is possible then that at this high flow condition the potential exists for higher damage rates than that found on the reference impeller. However, when considering the overall operating cycle for the full-scale

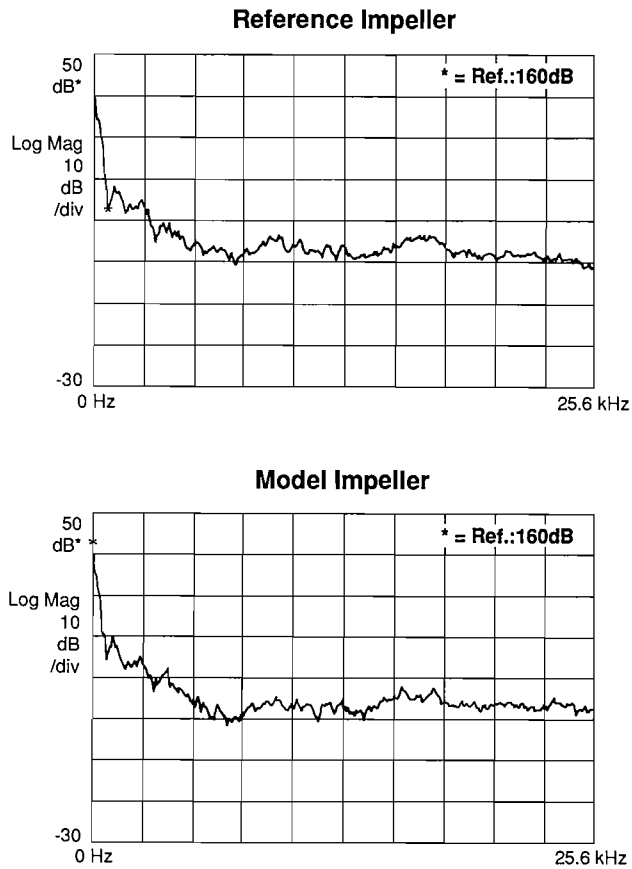


*Figure 19. Fluid-borne Noise Spectra for Reference and Model Impellers at 50 percent Flow. No noticable difference in noise spectra is observed between the two impellers in spite of the minimal cavitation activity found in the model Impeller. See Figures 11 and 12 for the cavitation activity measured by these two spectra.*

pump, it is unlikely that it will be required to spend 40,000 hr operating at 135 percent of rated flow. Over any realistic operating scheme, the authors still expect that life of the model (and production impeller) should far exceed 40,000 hr of cavitation life.

*Pressure Pulsations and Two-Phase Flow Interaction*

Aside from the impact of cavitation erosion on the mechanical integrity of the suction impeller, the next most influential two-phase flow phenomenon encountered during the comparative tests of the two impellers was subsynchronus pressure pulsation and the attendant vibratory response of the test pump. Observations from testing over the rated flow range at the supplied NPSHA produced no two-phase instability in the model impeller. This was expected, because the impeller operates either vapor free or (at the extremes of its operating range), nearly vapor free. The reference impeller did exhibit some measurable pulsations and vibration over the operating range, but not at levels which would cause concern. What both impellers exhibit is a rise in overall vibration levels as flow is reduced into the regime where suction recirculation exists.

It is interesting to note how these two designs respond to lower values of NPSHA than that supplied for this application. The lower dimensionless NPSH values ($\tau$) are often encountered in a variety of other applications, the most common being

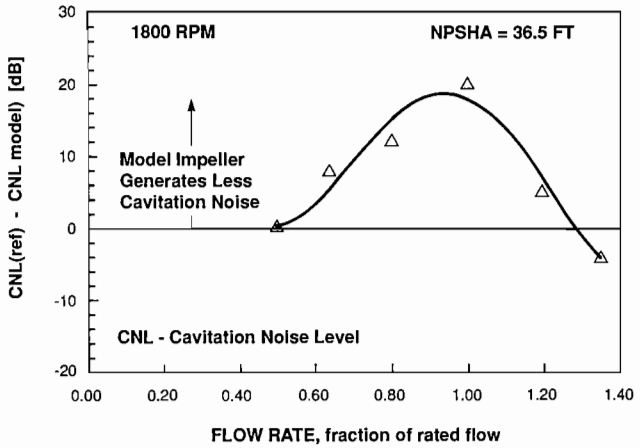


*Figure 20. Comparison of Broadband Cavitation Noise Levels. An 18-20 db reduction in cavitation noise level (CNL) is observed at the rated flow condition. Cavitation inception at 80 percent flow increases noise level even though no cavity is present. At maximum and minimum flow the noise levels of both impellers are nearly identical even though the amounts of vapor and damage potential are not necessarily equal.*

high-energy boiler feed service. The observations of the unsteadiness of the cavitating flow in these test impellers can be applied to these other applications.

The occurrence of subsynchronous pressure pulsations resulting from oscillating cavitation is most prevalent for the reference impeller. Pulsation and vibration data collected while operating this impeller at 80 percent of rated flow and at a τ-value of 0.28 are found in Figure 21. This flowrate is slightly greater than that for which the initiation of backflow was observed in the impeller passages. The NPSHA is near the NPSHR-value measured for this pump. This NPSHA (for three percent head drop) is somewhat higher than that found in most designs, because of the specific configuration of this particular side suction inlet. The top plot contains the spectrum of pressure pulsations measured in the suction bay. A subsynchronous pulsation was observed occurring at 8.5 hz (rotation frequency is 30 hz) and at an amplitude of about 3.0 psi peak to peak (1.5 psi half-amplitude). The nature of the pulsation affects more than the delivery of the pumped flow and head; it also affects the vibration signature of the pump casing as seen on the bottom trace of Figure 21. The time waveform of the inlet pressure transducer is shown on the bottom trace of Figure 22. This record encompasses approximately two seconds of time, or about 60 shaft revolutions.

A review of the video recording of the impeller inlet at this low-flow condition led to several observations regarding this behavior. By freezing the video and stepping frame by frame, it is apparent that the bubble lengths on each impeller vane change from one instant to another. The authors even observed that a blade may be completely free of any sheet cavity of measurable length. Further study of this video suggested that the phenomenon observed here is a rotating cavitation pattern in the impeller.

The influence of the oscillating cavitation on the vibration signature of the test rig was mentioned earlier. Four observations can be made upon inspection of the frequency plot of Figure 21:

• The rotation frequency of 30 hz (with a harmonic found at 60 hz) produces a casing velocity of 0.12 ips in amplitude. This is caused by unbalance (both mechanical and possibly hydraulic) and some misalignment of the test rig relative to its driver.

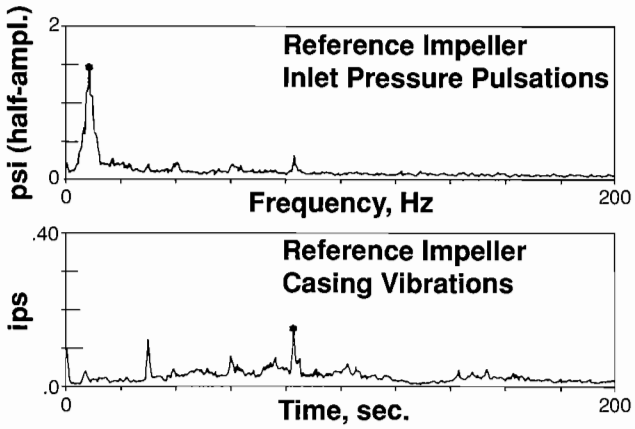


*Figure 21. Pressure Pulsation Activity of Reference Impeller and Test Rig Vibration at 80 percent Flow and Reduced NPSHA. The presence of a subsynchronous pressure pulsation shown here in the frequency domain, corresponds to the excitation of the natural frequency of the overhung rotor of the test rig.*

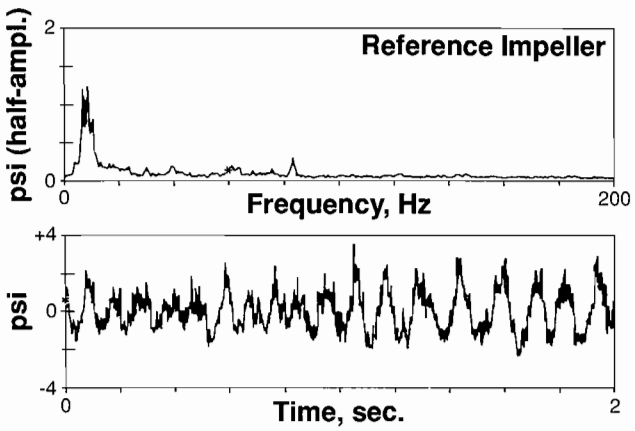


*Figure 22. Pressure Pulsation Activity of Reference Impeller at 80 percent Flow and Reduced NPSHA. Observation of the cavitation activity in the impeller suggests that the subsynchronous pulsation shown in the time waveform of this figure, is due to a rotating cavitation pattern, with each pressure excursion caused by the collapse of a vapor cavity on a blade surface.*

• A component of the vibration signature is found at 8.5 hz with an amplitude of less than 0.05 ips. This is the direct effect of the pressure pulsation on the mechanical system.

• The contribution at the vane pass frequency of 210 hz (not shown on this frequency scale) is small, with an amplitude of about 0.03 ips.

• The dominant vibration amplitude (0.15 ips) occurs at a frequency of 83-84 hz. This frequency is not an order of rotation frequency, and so further investigation was required to identify its source. The authors found that this frequency corresponds (within several hz) to the natural frequency of the overhung mass of the impeller on the pump shaft (which is supported by ball bearings; Figure 8.)

The correlation of the subsynchronous pressure pulsation activity with the vibration associated with the shaft natural

frequency became apparent once the pulsations and vibration had been mapped over the rated flow range together with a variation of NPSH. The results of this mapping are shown in Figure 23 for the reference impeller. A summary of the observations made from visual observations during the testing which produced the data for Figure 23 and comments on the data itself follow:

- Maximum pressure pulsation amplitudes occur at about 80 percent of rated flow.
- Pulsation amplitudes were attenuated below 80 percent flow. Recirculation was observed in the impeller passages at 75 percent flow.
- Frequency of the pulsation is influenced most by NPSH.
- Maximum pulsation amplitudes occur at the flowrate where cavity length is at a maximum (Figure 5).
- Maximum rotor vibration also occurs at 80 percent of design flow, but at a higher NPSH than that of the maximum pulsation condition.
- Visual perception of oscillating cavitation is strongest at 80 percent flow.

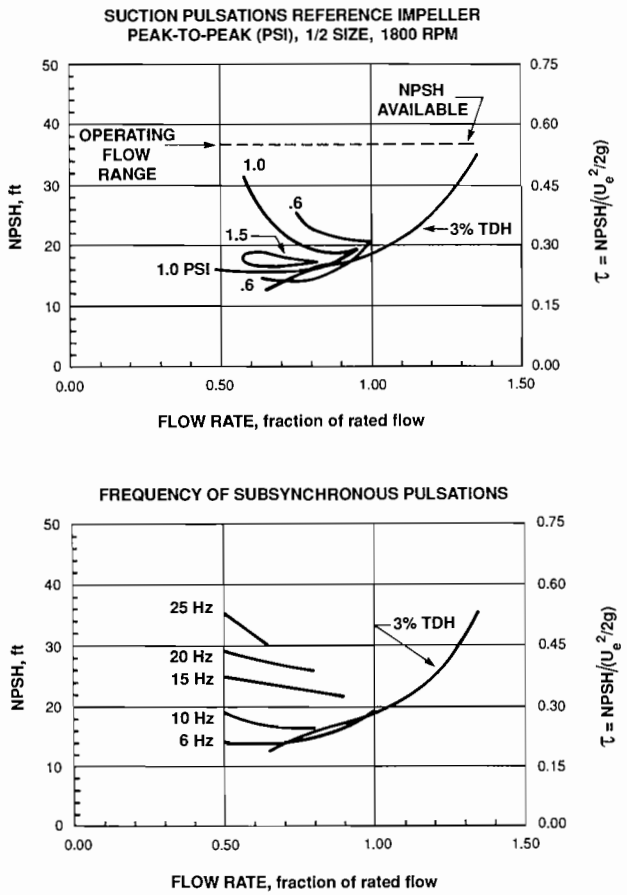


*Figure 23. Pressure Pulsation Amplitudes, Frequencies and Casing Vibration Measured with the Reference Impeller. The subsynchronous pulsations observed are most severe near the 80 percent flow condition and are found to attenuate as flow is reduced, and suction recirculation effects become dominant. Frequency (middle plot) varies with NPSHA. Vibration amplitudes resulting from the suction instablity and occurring at 84 hz are displayed on the bottom plot.*

The instability identified as oscillating cavitation (or actually a rotating pattern of cavitation) is inherently a high flow phenomenon, as it is connected with cavity instability. (At lower flowrates the *cavity* disappears.) For the reference impeller this translates to flows greater than 75 percent of design. The pulsations and resulting mechanical interaction are reduced as flow is decreased into the region where suction recirculation effects become more influential. The region between 80 percent and 50 percent flow appears to be a transition zone between well ordered approach flow (>75 percent flow) and the deep suction recirculation encountered at at flows less than 50 percent of design. In the low flow regime, the influence of the swirling backflow on the incoming flow dominates the impeller inlet and prevents any orderly formation of suction side vapor cavities. The behavior in this regime has been described in literature for a variety of pumps which include high specific speed axial inducers, side-suction approach boiler feed pumps, and end suction volute pumps [7, 8].

The plots of pressure pulsation and casing vibration found in Figure 24 (for the model impeller) should be compared with Figure 21 (reference impeller). A subsynchronous pulsation is present, although at a reduced amplitude (1.0 psi vs. 3.0 psi) and at an increased frequency (12.5 hz vs 8.5 hz). This pulsation was not capable of exciting the rotor vibration found during operation of the reference impeller. The only significant component of the vibration spectrum for this condition occurs at

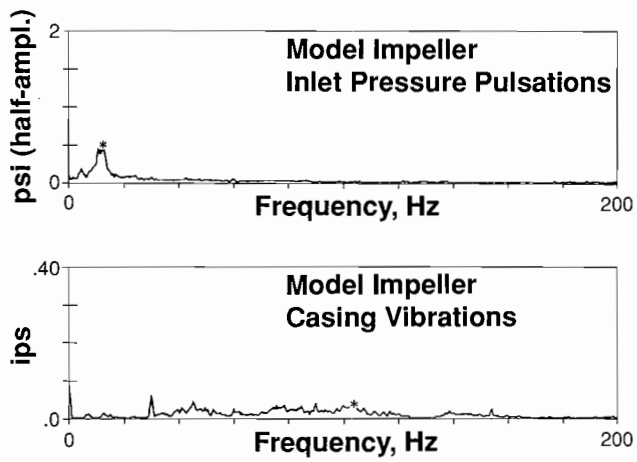


*Figure 24. Pressure Pulsation Activity of Model Impeller and Test Rig Vibration at 80 percent Flow and Reduced NPSHA. Suction pulsations and casing vibration are displayed here in the frequency domain. Less vapor present in the model impeller at this condition than in the reference impeller. Therefore, the amplitude of the subsynchronous pulsation is less and of a higher frequency. No excitation of the rotor was found at this condition.*

rotation frequency of 30 hz. A complete mapping of pulsation activity and frequency content for the model impeller appears in Figure 25. The influence of suction recirculation on the subsynchronous pulsations is still apparent (although the onset of recirculation in the impeller passages occurs at a about 65 percent flow as opposed to 75 percent flow on the reference impeller). For the model impeller, the pulsation amplitudes are lower and the frequency of occurrence is higher. This is attributed to the major reduction in cavity volume achieved from the improved design approach used on this impeller.

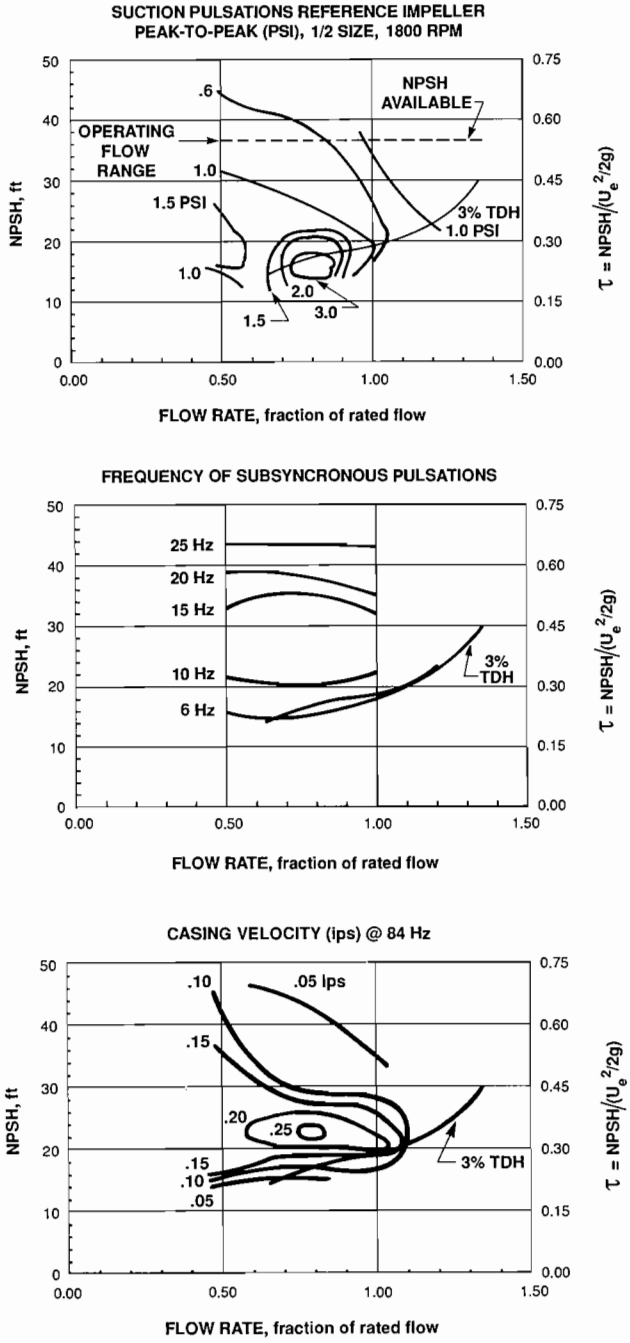


*Figure 25. Model Impeller Pressure Pulsation Activity. The model impeller has less subsynchronous pulsation activity than does the reference impeller because of the reduced cavity volumes, which are also accociated with higher frequencies at the same NPSHA. No significant vibration was detected on the bearing housing.*

## CONCLUSIONS

The design of the suction stages of a 22,000 hp high energy pipeline pump was examined in a half-scale model test program. It was established that the model impeller would suffer significantly less from cavitation erosion and cavitation related instablility than a reference impeller which was supposed to be capable of surviving cavitation attack for 40,000 hr of pump operation.

The reference impeller was designed according to a procedure that had evolved from extensive studies of field experience, and consisted mainly in correctly matching the inlet eye and blade leading edge angles to the incoming flow—over the specified operating flowrate range.

The model impeller, which was compared with the reference impeller, carried this design approach a step further. The blades were specially shaped in the leading edge region to maintain the suction side pressure at a level above the vapor pressure. That this condition was met was analytically verified via the use of NASA-developed quasi-three dimensional computer codes.

In the model testing, the impellers were compared via visualization of the cavitating flow in the inlet regions, removal of soft coating caused by such flow, cavitation noise level and pressure pulsation activity. In each of these comparative approaches, the model impeller showed the expected improvement arising from the stated design process. There was no difference in hydraulic performance over the specified flow range from 50 percent to 135 percent of the rated flow, except that above 120 percent the model impeller experienced an increase in the NPSH required to maintain head (NPSHR), but this NPSHR was still less than the available NPSH.

In terms of the flow visualization results, while there was a moderate amount of two-phase activity within the reference impeller that should be compatible with the 40,000-hr life requirement for the given available NPSH, the model impeller, on the other hand, showed a complete absence of cavitation activity over a flow range from 80 percent to 120 percent of the rated condition, at this same NPSH. Furthermore, this impeller showed significantly less bubble activity over the whole flow range from 50 percent to 135 percent of rated than did the reference impeller.

As a result of the absence of cavities in the stated flow range, the cavitation noise level of the model impeller was less (by as much as 20 dB) than it was for the reference impeller. This was true throughout the specified flow range, except that at flows above 128 percent of rated, the model showed a slightly higher cavitation noise level. For a typical operating cycle, however, the model impeller clearly has a greater resistance to cavitation erosion. This conclusion is reinforced by the fact that the model impeller suffered less removal of soft coating (stencil ink) as a consequence of the observed cavitation patterns.

The most significant benefit of the design process used for the model impeller was the virtual elimination of pressure pulsations and the attendant mechanical response of the pump test rig that routinely accompany the existence of significant vapor volume within an impeller. Characaterized as "oscillating cavitation," this phenomenon was eliminated in the flow range for which no cavitation was observed in the model impeller. At the other flows outside this range, these disturbances were relatively insignificant.

The authors conclude that the stated analytically based design procedure for the cavitation-sensitive inlet regions of pump impellers is beneficial in achieving improved, reliable performance of the suction stages of high energy centrifugal pumps. Further, through the use of flow visualization and ancillary testing, the useful range of performance of such pumps can be established.

## APPENDIX

### *Fluctuating Radial Loads Arising from Oscillating Cavitation*

Fluctuating axial and radial loads, as well as a tilting moment, can arise from oscillating cavities in a centrifugal pump impeller. To illustrate the character of this hydraulic mechanical

interaction, now look at the radial load. In this case, the average value of the fluctuating stress, $s_{brgs}$ in journal-type radial bearings supporting the impeller is

$$S_{brgs} = [\Delta P_{stg}\, k_h\, k_a \cdot (b_2 + 2b_{sh}) \cdot D_2]/(D_s \cdot \Sigma l_{brg}) \qquad (A1)$$

where $\Delta P_{stg}$ = pump pressure rise
$k_h$ = fraction of $\Delta P$ that is momentarily lost because of the extension of an oscillating cavity into the affected impeller passage(s)
$k_a$ = fraction of the impeller outside diameter $D_2$ (projected radially) that is subjected to the unbalanced radial load $k_h\, \Delta P_{stg}$
$b_2$ = impeller exit blade width
$b_{sh}$ = shroud thickness at (closed) impeller exit
$D_2$ = impeller outside diameter
$D_s$ = shaft journal diameter
$\Sigma l_{brg}$ = sum of the axial lengths of the bearings

The geometric ratio $b_2/d_2$ is typically optimized for each value of the specific speed, $\Omega_s$ where

$$\Omega_s = \Omega Q^{1/2}/(\Delta P/\rho_L)^{3/4} \qquad (A2)$$

with $Q$ = pump flow flow rate
$\Omega$ = angular speed of pump
$\rho_L$ = density of pumped liquid.

Since $Q = V_{m,2}\, \pi\, D_2\, b_2$, Equation (A2) can also be written in terms of $b_2/D_2$; i.e.,

$$\Omega_s = [4\pi\phi_2(b_2/D_2)]^{1/2}/\psi^{3/4} \qquad (A3)$$

where the impeller exit flow coefficient

$$\phi_2 = V_{m,2}/U_2 \qquad (A4)$$

with $V_{m,2}$ = the meridional (radial in this case) component of the fluid velocity
$U_2 = \Omega r_2$ = impeller tip speed at the outer diameter
and the head coefficient

$$\psi = (\Delta P/\rho_L)/U_2^2 \qquad (A5)$$

Since $\phi$ and $\psi$ are also typically optimized vs specific speed, we can eliminate them with the following fits to Stepanoff's data (*22*):

$$\phi = 0.1715\Omega_s^{1/2} \qquad (A6)$$

and

$$\psi = 0.383/\Omega_s^{1/3} \qquad (A7)$$

Now we can rewrite Equation (A1) as follows:

$$s_{brgs} = (\Delta P - fct) \cdot [0.11111 + (N_s/8946)] \qquad (A8)$$

where

$$(\Delta P - fct) = \Delta P_{stg} \cdot \left[ \frac{k_h \cdot (k_a/0.5)}{\left(\frac{\Sigma l_{brg}/D_s}{2.0}\right) \cdot \left(\frac{D_s/D_2}{0.3}\right)^2} \right] \qquad (A9)$$

$N_s$ = specific speed in U.S. units (rpm, USgpm, ft)
$= \Omega_s \cdot 2733$,

and we have taken $b_{sh} = 0.02\, D_2$.

The quantity in brackets in Equation (A9) is perhaps typically equal to unity. More precisely, however, the magnitudes and frequencies of $k_h$ and $k_a$ are fundamentally dependent on the flowrate fraction $Q/Q_{bep}$ and the cavitation coefficient $\tau = NPSH/(\Omega^2 r^2/2g)$. While the character of these particular dependencies needs further study, one can get an idea of the behavior of $k_h$ by referring to Figures 23 and 25 of this paper. A plot is shown in Figure 1 of Equation (A8) solved for $\delta$P-fct vs $N_s$ as a function of $s_{brgs}$, which is the average zero-to-peak amplitude of the fluctuating stresses arising in the radial bearings of the pump through oscillating cavitation.

## NOMENCLATURE

| | |
|---|---|
| A | fluid correction factor in erosion equation (7) |
| $b_{sh}$ | width of impeller at outlet, including shrouds |
| $b_2$ | width of impeller flow passage at outlet |
| BEP | best efficiency point |
| C | blade-side erosion constant in Eq. (7) |
| $C_a$ | specific speed-effect constant in Eq. (5) |
| $C_b$ | fluid vaporization-effect constant in Eq. (5) |
| $C_c$ | constant for the material of construction - Eq. (5) |
| $C_p$ | pressure coefficient - defined in Eq. (10) |
| $D_e$ | impeller eye diameter (i.e., at the shroud at inlet) |
| $D_s$ | minimum diameter of flow passage at impeller inlet eye |
| $D_2$ | impeller mean outlet diameter |
| E | erosion depth at point of maximum cavitation attack |
| f | off-design function in Eq. (6) |
| g | acceleration of gravity |
| H | pump head |
| $K_1, K_2, \ldots, K_5$ | constants in minimum flow eq. (3) |
| $k_A$ | cavitation number defined in Eq. (7) |
| $k_a$ | impeller projected area constant in Eq. (A1) |
| $k_h$ | fraction of pressure rise in Eq. (A1) |
| $k_1$ | entrance coefficient in $NPSH_{40}$ - Eq. (5) |
| $k_2$ | blade pressure drop coefficient in $NPSH_{40}$-eq. (5) |
| $L_{cav}$, $L_{cav.ref}$ | cavity lengths in erosion eq. (7) |
| $l_{brg}$ | axial length of journal bearing in Eq. (A1) |
| N | rotative speed |
| NPSH | net positive suction head |
| NPSHA | available NPSH |
| NPSHR | NPSH required to limit head reduction due to cavitation to 3% of H |
| $N_s$ | specific speed of pump stage in U.S. units (rpm, gpm, ft) |
| n | exponent in erosion eq. (7) |
| P | total pressure |
| $P_o$ | total pressure at pump inlet |
| p | static pressure |
| $p_v$ | vapor pressure of the pumped liquid |
| Q | volume flow rate |
| $Q_{bep}$ | Q at the best efficiency point |
| $Q_{ma}$ | minimum allowable flow rate defined in Eq. (3) |
| $Q_{max}$ | required maximum flow rate (Table 1) |
| $Q_{min}$ | required minimum flow rate (Table 1) |
| $Q_r$ | rated flow |
| R | ratio of NPSHA to NPSHR |
| r | radius |
| $r_e$ | impeller eye radius (half of $D_e$) |
| $s_{brgs}$ | average unit load in journal bearings |
| t | time |
| TS | tensile strength |
| $U_e$ | impeller inlet tip speed |
| $V_{m,2}$ | meridional (essentially radial) velocity component at the outlet of impeller |

| | |
|---|---|
| $\beta_e$ | blade leading edge camberline angle at the shroud |
| $\rho_L$ | density of the pumped liquid |
| $\tau$ | NPSH-coefficient or dimensionless NPSH ($=2gNPSH/U_e^2$) |
| $\phi$ | inlet flow coefficient - defined in Table 2 |
| $\psi$ | impeller head coefficient - defined in Eq. (A5) |
| $\Omega$ | angular speed of impeller or pump |
| $\Omega_s$ | universal specific speed - defined in Eq. (A2) ($=N_s/2733$) |

*Subscripts*

| | |
|---|---|
| A | related to available NPSH (i.e., to NPSHA) |
| bep | at best efficiency point |
| se | at shockless entry flow rate |
| sr | at the flow rate where fluid begins to recirculate out of the impeller eye; i.e., the point of suction recirculation |

## REFERENCES


1. Cooper, P., Wotring, T., Makay, E., and Corsi, L., "Minimum Continuous Stable Flow in Feed Pumps," Symposium Proceedings: Power Plant Pumps, EPRI CS-5857, pp. 2-97 to 2-132 (June 1988).
2. Cooper, P., and Antunes, F. F., "Cavitation in Boiler Feed Pumps," Symposium Proceedings: Power Plant Feed Pumps - The State of the Art, EPRI CS-3158, pp. 2-24 to 2-49 (July 1983).
3. Gulich, J. F., "Guidelines for Prevention of Cavitation in Centrifugal Feed Pumps" EPRI GS-6398 (November 1989).
4. Brennen, C., and Acosta, A. J., "The Dynamic Transfer Function for a Cavitating Inducer," Transactions of ASME, Journal of Fluids Engineering, 98, pp. 182-191 (1976).
5. Palgrave, R., and Cooper, P., "Visual Studies of Cavitation in Pumping Machinery," Proceedings of the 3rd International Pump Symposium, Turbomachinery Laboratory, Department of Mechanical Engineering, Texas A&M University, College Station, Texas, pp. 61-68 (1986).
6. Cooper, P., "Hydraulics and Cavitation," Symposium Proceedings: Power Plant Pumps, EPRI CS-5857, pp. 4-109 to 4-149 (June 1988).
7. Sloteman, D. P., Cooper, P., and Dussourd, J. L., "Control of Backflow at the Inlets of Centrifugal Pumps and Inducers," Proceedings of the First International Pump Symposium, Turbomachinery Laboratory, Department of Mechanical Engineering, Texas A&M University, College Station, Texas, pp. 9-22 (May 1984).
8. Kasztejna, P. J., Heald, C. C., and Cooper, P., "Experimental Study of the Influence of Backflow Control on Pump Hydraulic-Mechanical Interaction," Proceedings of the Second International Pump Symposium, Turbomachinery Laboratory, Department of Mechanical Engineering, Texas A&M University, College Sstation, Texas, pp. 33-40, (April 1985).
9. Hallam, J. L., "Centrifugal Pumps: Which Suction Specific Speeds are Acceptable," Hydrocarbon Processing (April 1982).
10. Vlaming, D. J., "Optimum Impeller Inlet Geometry for Minimum NPSH Requirements for Centrifugal Pumps," Pumping Machinery - 1989, ASME, pp. 25-29 (July 1989).
11. Cooper, P., "Application of Pressure and Velocity Criteria to the Design of a Centrifugal-Pump Impeller and Inlet," Transactions of ASME, Journal of Engineering for Power, 86, pp. 181-190 (April 1964).
12. Katsanis, T., and McNally, W. D., "Revised Fortran Program for Calculating Velocities and Streamlines on the Hub-Shroud Midchannel Stream Surface of an Axial-, Radial-, or Mixed-Flow Turbomachine or Annular Duct," NASA TN D-8430 and D-8431 (1977).
13. Katsanis, T., "Fortran Program for Calculating Transonic Velocities on a Blade-to-Blade Stream Surface of a Turbomachine," NASA TN D-5427 (1969).
14. Gopalakrishnan, S., "A New Method for Computing Minimum Flow," Proceedings of the 5th International Pump Users Symposium, Turbomachinery Laboratory, Department of Mechanical Engineering, Texas A&M University, College Station, Texas, pp. 41-47 (May 1988).
15. Fraser, W. H., "Recirculation in Centrifugal Pumps," Materials of Construction of Fluid Machinery and Their Relationship to Design and Performance, ASME, pp. 65-86 (1981).
16. Singh, P. J., "Cavitation Damage Rate Investigation," PRADCO Annual Report, R3-03, Task 3 on EPRI Contract RP1884-18 (January 1989).
17. Cooper, P., Singh, P. J., and Sloteman, D. P., "A New Replica Method for Measuring Cavitation Damage," Cavitation and Multiphase Flow Forum-1987, ASME Book No. H00382 (1987).
18. Ruggeri, R. S., "Experimental Studies on Thermodynamic Effects of Developed Cavitation," Fluid Mechanics, Acoustics, and Design of Turbomachinery, NASA SP-304, Part I, pp. 377-401 (1974).
19. Cooper, P., "Analysis of Single and Two-Phase Flows in Turbopump Inducers," Transactions ASME, Journal of Engineering for Power, 89, pp. 577-588 (October 1967).
20. Schiavello, B., Arisawa, T., and Marenco, G., "Flow Visualization—A Design Tool to Improve Pump Cavitation Performance," presented at the Second International Symposium on Transport Phenomena, Dynamics and Design of Rotating Machinery, ASME, Honolulu, Hawaii (April 1988).
21. McNulty, P. J., and Pearsall, I. S., "Cavitation Inception in Pumps," Transactions of ASME, Journal of Fluids Engineering, Vol 104, March 1982, pp. 99-104.
22. Stepanoff, A. J., Centrifugal and Axial Flow Pumps, 2nd Edition, New York, New York: John Wiley & Sons, p. 176 (1967).


## ACKNOWLEDGEMENTS

The authors extend their appreciation to all who participated in formulating the concepts, gathering data and generally supporting the program presented. In particular, we thank the management of the Ingersoll-Rand Company and especially Walter J. Schmidt for his long-term commitment and support of the dedicated research laboratory and personnel involved. Kim Horten conducted the tests and obtained much of the data; and T. L. Wotring, C. Hay, G. J. Slaghekke and several others provided continual support, interest and direction during the progress of the work reported herein.